

Radiopurity measurements of liquid scintillator for the COSINE-100 Upgrade

J. Kim^a C. Ha^{a,1} S.H. Kim^b W.K. Kim^{c,b} Y.D. Kim^{b,c} Y.J. Ko^{b,2} E.K. Lee^b H. Lee^{c,b}
H.S. Lee^{b,c} I.S. Lee^b J. Lee^b S.H. Lee^{b,c} S.M. Lee^d Y.J. Lee^a G.H. Yu^{e,b}

^a*Department of Physics, Chung-Ang University,
Seoul 06974, Republic of Korea*

^b*Center for Underground Physics, Institute for Basic Science(IBS),
Daejeon 34126, Republic of Korea*

^c*IBS School, University of Science and Technology (UST),
Daejeon 34113, Republic of Korea*

^d*Department of Physics and Astronomy, Seoul National University,
Seoul 08826, Republic of Korea*

^e*Department of Physics, Sungkyunkwan University,
Suwon 16419, Republic of Korea*

E-mail: chha@cau.ac.kr, yjko@ibs.re.kr

ABSTRACT: A new 2,400 L liquid scintillator has been produced for the COSINE-100 Upgrade, which is under construction at Yemilab for the next COSINE dark matter experiment phase. The linear-alkyl-benzene-based scintillator is designed to serve as a veto for NaI(Tl) crystal targets and a separate platform for rare event searches. We measured using a sample consisting of a custom-made 445 mL cylindrical Teflon container equipped with two 3-inch photomultiplier tubes. Analyses show activity levels of 0.091 ± 0.042 mBq/kg for ^{238}U and 0.012 ± 0.007 mBq/kg for ^{232}Th .

KEYWORDS: Liquid Scintillator, Dark Matter, Radiopurity

¹Corresponding author.

²Corresponding author.

Contents

1	Introduction	1
2	Experimental setup for radiopurity measurements	2
3	Detector response	2
3.1	Particle identification	2
3.2	Energy calibration	3
4	Coincidence analysis	5
4.1	$\beta - \alpha$ from ^{238}U chain	5
4.2	$\alpha - \alpha$ from ^{232}Th chain	6
5	Summary and discussion	7

1 Introduction

Observational evidences for the existence of dark matter has been well-documented [1–3], leading to a surge in direct detection experiments [4]. Among these, the DAMA experiment has claimed the observation of an annual modulation signal that aligns with the presence of weakly interacting massive particles (WIMPs), a leading dark matter candidate [5, 6]. To independently test the DAMA experiment, the COSINE experiment was launched, using the same target material, NaI(Tl) crystals [7]. After 6.5 years of operation at the Yangyang Underground Laboratory, the COSINE-100 experiment has produced results that challenge DAMA’s claims with a significance of over 3 standard deviations [8]. Preparations are now underway for the next phase, the COSINE-100 Upgrade (COSINE-100U) [9], at a new underground facility, Yemilab, in Jeongseon, Korea [10].

The COSINE-100 experiment installed a unique liquid scintillator (LS) system to help characterize signals and backgrounds in the crystals. The same system will be used in the upcoming COSINE-100U experiment. The NaI(Tl) crystal assemblies are positioned at the center of an acrylic box, which is filled with 2,400 liters of LS, ensuring a minimum thickness of 40 cm of LS surrounding the crystal assembly at all points. Eighteen 5-inch PMTs (R877-100) attached to the box record light signals produced in the LS, and data acquisition system combine simultaneously those with the crystal signals. Thus, the LS functions as a tagger for gamma rays originating both from outside the box and from the crystals themselves. The LS veto system has demonstrated tagging efficiencies of 15–30% in the 2–6 keV range, with 65–75% efficiency for the detection of ^{40}K originating from the crystals [11]. The tagged events can also serve as independent channel for understanding the background [12]. Additionally, the LS is utilized for exotic dark matter searches when the coincidence interactions occur.

A total of 2,400 liters of the linear alkylbenzene (LAB) based LS has been produced and is awaiting use in the COSINE-100U experiment. Three grams of 2,5-diphenyloxazole (PPO) were added per liter of LAB to act as a fluorescent material. Since the emission spectrum of PPO does not match the spectral response of the PMT, 30 mg/L of 1,4-bis[2-methylstyryl]benzene (bis-MSB) was added as a wavelength shifter for efficient light collection [13].

The radiopurity of the LS was measured prior to installation in the main detector to minimize the risk of introducing significant background radioactivity to the crystals. Data was collected for a month with a small detector at a ground laboratory. The data was subjected to pulse shape discrimination (PSD) and β/α coincidence analysis to determine the internal background level. Additionally, radioactivity measurements of the LS sample were performed using high-purity germanium detectors [14] for comparison.

2 Experimental setup for radiopurity measurements

To measure radiopurity, a detector designed to hold a 445 mL LS sample was built. As shown in Fig. 1 (a), a Hamamatsu R12669SEL¹ PMT was installed in each of two PTFE cases, designed so that the space between them is filled with LS. The inner radius of the case exactly matches the PMT radius to secure PMTs and prevent leakage through the gap between the case and PMTs. The outer radius of the case is 7.6 cm, and there are six 3 mm radius holes that go through the cases as shown in Fig. 1 (a) and (b). When the two PTFE cases are joined, an O-ring is placed at the matching area, and long bolts are inserted into the six holes, with nuts tightened on the outside of the cases. The LS is introduced through the chimney.

The assembled detector was shielded with lead bricks to reduce external background, as shown in Fig. 1 (c). An additional layer of polyethylene blocks was added for environmental neutron shielding (see Fig. 1 (e)). The analog signal pulses were digitized and recorded using analog-to-digital converter (ADC) modules with a 2 ns sampling rate. An event was triggered only when both PMT signals exceeded 6 mV discrimination. With a trigger rate of 6 Hz, a total of 522 hours of data was collected over the course of a month.

3 Detector response

3.1 Particle identification

Pulse shape discrimination (PSD), which distinguishes between β/γ and α/n^0 based on the decay time of the LS, is a popular technique for particle identification (PID). To identify the difference in decay time from the waveform, a PSD parameter is defined as the ratio of two variables, Q_{tail} and Q_{total} ,

$$\frac{Q_{\text{tail}}}{Q_{\text{total}}} = \frac{\sum_{t_E-t_c}^{t_E} q_i}{\sum q_i}, \quad (3.1)$$

where t_c is the range of summation for Q_{tail} , while t_E and q_i are the end time bin and the charge of i^{th} bin in the waveform, respectively. Figure 2 (a) shows the distribution of PSD parameter when t_c is 30 ns. One can see the β/γ events distributed from 0.07 to 0.12 while α/n^0 events are distributed

¹selected for high quantum efficiency

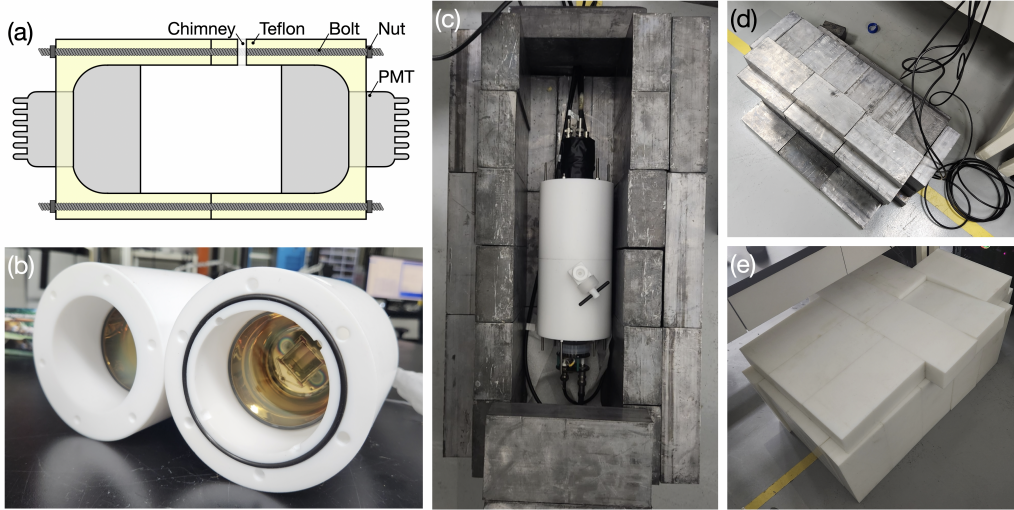


Figure 1. (a) The schematic of the detector. (b) Cross section of the detector. (c) Detector assembly in the lead castle. (d) Lead shielding from the outside. (e) PTFE shielding from the outside.

from 0.14 to 0.18. The decay time of β/γ events is relatively short, and thus appear in the lower range of PSD parameter, while α/n^0 is distributed in the higher range.

Each distribution was modeled as a Gaussian distribution through fitting, and the β/γ and α/n^0 distributions are colored blue and red, respectively, in the figure. The discriminative power of the PSD parameter can be quantified by the figure of merit (FoM), which is defined as follows,

$$\text{FoM} = \frac{\mu_{\alpha/n^0} - \mu_{\beta/\gamma}}{\sqrt{\sigma_{\alpha/n^0}^2 + \sigma_{\beta/\gamma}^2}}, \quad (3.2)$$

where μ and σ are the mean and standard deviation of the Gaussian functions, respectively. Since the FoM depends on the t_c , for optimization we scan the FoM by varying the t_c within 5 to 30 time bins, corresponding to 10 to 60 ns. Figure 2 (b) shows the scan results of the FoM as t_c varies. We determined t_c to be 30 ns with the largest FoM value.

The charge-dependent distribution of the PSD parameter with optimized t_c can be seen in Fig. 3. One can see a clear distinction between the β/γ and α/n^0 bands based on the red curve, and the three islands in the α/n^0 band represent α events. To determine the criteria for α/n^0 selection, the data was divided into nine zones based on charge sum, from 6,000 ADC to 24,000 ADC. For each zone, the PSD parameter distribution was fitted with two Gaussian functions, and then we found a cut value that rejects 99.87% of β/γ events. These cut values are plotted in Fig. 3 as pink dots, and a linear function was obtained by fitting them to use as a selection criterion. Here, the PSD cut shows an efficiency of over 94.51% for α/n^0 events over 10,000 ADCs.

3.2 Energy calibration

The three islands identified in Fig. 3 appear as three distinct peaks in the charge distribution of the α/n^0 events selected via PID in Sec. 3.1 as shown in Fig. 4 (a). They appear to come from α peaks caused by ^{222}Rn contaminated during LS production and detector assembly, and the charge ratios

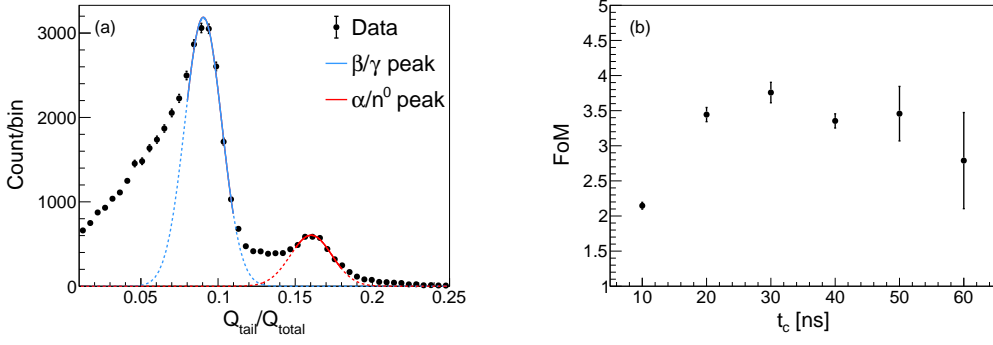


Figure 2. Q_{tail} optimization. As varying the t_c from 10 ns to 60 ns, draw the PSD parameter distribution as (a) and fit it with Gaussian function (blue and red curve). FoM between the β/γ and α/n^0 can be decided from the fitting, and is shown on (b). The highest FoM is 3.8σ when t_c is 30 ns.

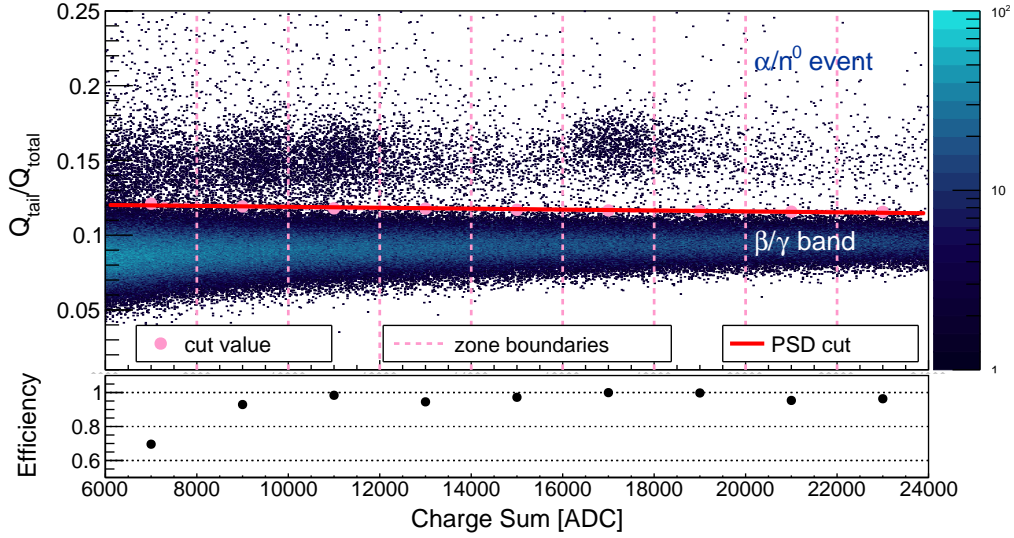


Figure 3. Pulse shape discrimination between β/γ and α/n^0 events. The clear band below the red line shows the distribution of β/γ events, while the band with three islands above the curve shows the distribution of α/n^0 events. The red line was used to separate α/n^0 events from β/γ events.

between them are in good agreement with the ratios between the α decay energies of ^{222}Rn , ^{218}Po , and ^{214}Po which allows for an α energy calibration.

The charge distribution of the α/n^0 events was modeled with three Gaussian functions to describe the three α peaks and one exponential function to account for the background consisting mainly of fast neutrons. The red solid line in Fig. 4 (a) indicates the fitted model, and one can see the three Gaussian peaks represented by the dashed lines. The means and standard deviations of the Gaussian functions were used to determine the calibration and resolution functions for α energy.

In Fig. 4 (b) and (c), the black dots with error bars were obtained from the fitting results with known energies of three α peaks. The mean charge was fitted by a linear function and used as an

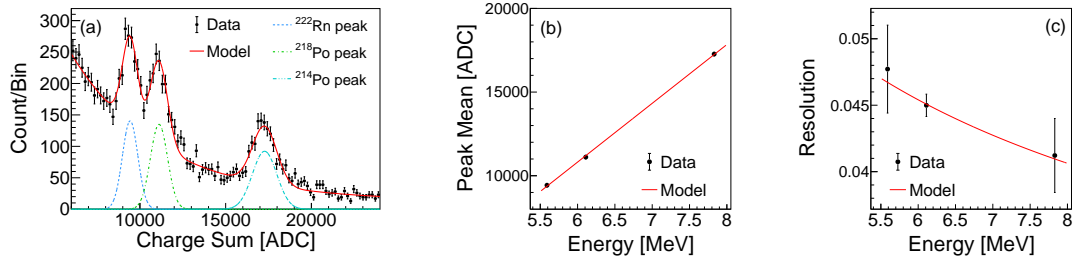


Figure 4. Energy Calibration. (a) Two Gaussian function with exponential component for background were used to fit the ^{222}Rn and ^{218}Po peaks that shown on lower energy range. For the fitting, three Gaussian function with exponential term and constant term was used. Total three means and three widths of each peaks were obtained and these are used for the energy calibration function (b) and the resolution function (c).

calibration function for α energy, while the resolution was fitted by,

$$\frac{\sigma_E}{E} = \sqrt{\frac{A}{E} + B}, \quad (3.3)$$

where σ_E is the energy resolution, while A and B are used as fitting parameters. The fitted functions for α energy calibration and resolution are shown as red solid lines in Fig. 4 (b) and (c), respectively.

4 Coincidence analysis

4.1 $\beta - \alpha$ from ^{238}U chain

To measure the activity of the LS-contaminated ^{238}U series, the decays of ^{214}Bi and ^{214}Po in the decay chain were investigated. The isotope ^{214}Bi produces ^{214}Po via β -decay with a Q-value of 3.27 MeV. The isotope ^{214}Po then undergoes α -decay with a Q-value of 7.83 MeV and a half-life of 164.3 μs to produce ^{210}Pb . Thanks to the short decay time of ^{214}Po , these sequential decays can appear as a time-coincidence event.

Utilizing the PID from Sec. 3.1, the time difference between β and α over a range of 2 to 1000 μs is shown in Fig. 5 (a). When $\beta - \alpha$ time difference is between 2 and 1,000 μs , the energy distribution of those coincident α events is represented by the red-filled histogram in Fig. 5 (b). The coincidence time between β and α events can be determined by fitting the data with an exponential function. Since random coincidences between β/γ and α/n^0 events may occur, we used an exponential function with an added constant term,

$$f(\Delta t) = A \exp\left(-\frac{\Delta t}{t_{1/2}/\ln 2}\right) + C, \quad (4.1)$$

where the variable Δt is time difference between β/γ and α/n^0 . The three fitting parameters are A , $t_{1/2}$, and C . Here, A represents the activity of ^{210}Po , $t_{1/2}$ is its half-life, and C accounts for the amount of random coincidence. We obtained the best-fit half-life of $160.1 \pm 5.1 \mu\text{s}$, which is consistent with the known value.

A significant portion of the remaining $\beta - \alpha$ time-coincidence events is attributed to contamination from ^{222}Rn (with a half-life of 3.8 days). Consequently, it is necessary to analyze these

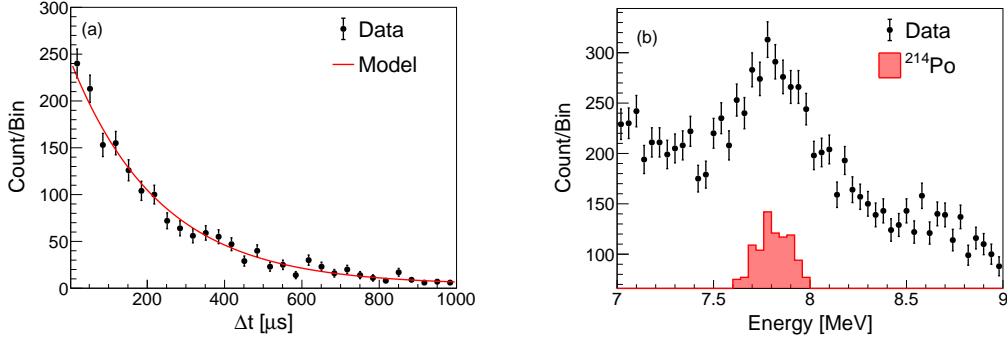


Figure 5. Sequential decays of ^{214}Bi and ^{214}Po tagged via $\beta - \alpha$ time coincidence. (a) Time difference between β and α events to tag the sequential decays of ^{214}Bi - ^{214}Po (black dots with error bars). The red curve is a function fitted to the data. (b) The energy distribution α/n^0 identified by PSD in Sec. 3.1. The black dots denotes total α/n^0 events, while the red-filled histogram represents the α events from ^{214}Po decay.

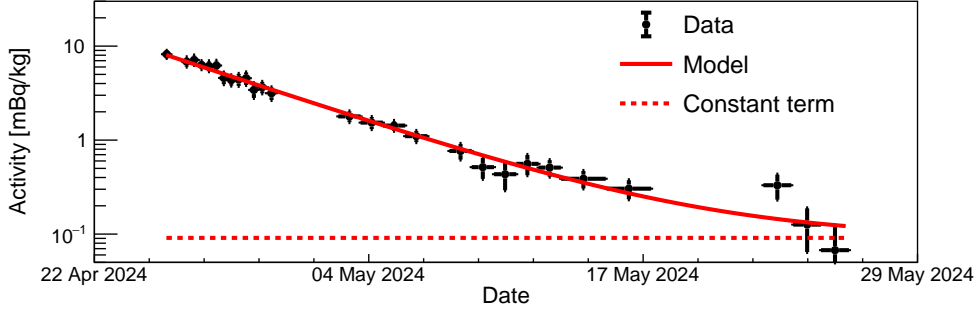


Figure 6. The value and error of the activity obtained from the data in each time interval are shown as black dots and error bars, respectively. They were fitted with a function represented by the red solid line, of which the constant term is depicted by the red dashed line.

events over an extended period. The collected data over a month were divided into appropriate time intervals for this analysis. The Δt distribution in each interval was fitted by Eq. 4.1 with the half-life fixed at $164.3 \mu\text{s}$, while keeping A and C as free parameters.

The activity A , determined from the fitting, is plotted as black dots with error bars in Fig. 6. The observed decrease in activity appears to be due to contamination from ^{222}Rn prior to detector assembly. To model this decrease, we used the same function as in Eq. 4.1. The exponential term represents the contribution from ^{222}Rn , while the constant term accounts for internal contamination from the ^{238}U series. The best-fit model, shown by the solid red line, aligns well with the observed decrease in activity. The internal contamination from ^{238}U , as determined from the constant term, is $0.091 \pm 0.042 \text{ mBq/kg}$.

4.2 $\alpha - \alpha$ from ^{232}Th chain

The sequential α decays of ^{220}Rn and ^{216}Po in the ^{232}Th decay chain can be identified by time-coincidence condition, thanks to the short ^{216}Po 's half-life of 140 ms. A dataset consisting of

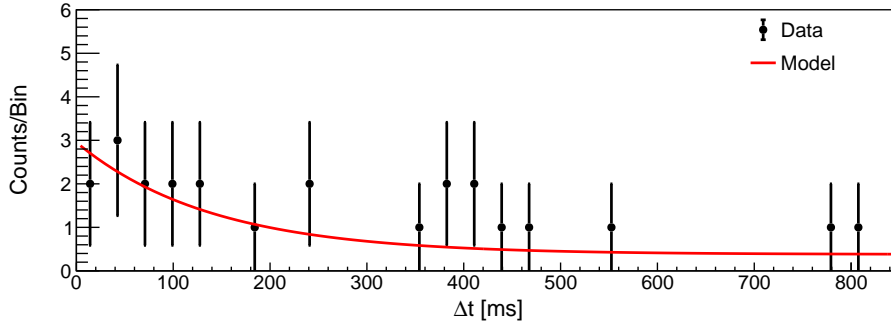


Figure 7. The $\alpha - \alpha$ coincidence events by a sequential decays of ^{220}Rn and ^{216}Po . Time differences between coincidence α events are denoted by black dots with error bars, while the red line indicates the fitted function using Eq. 4.1.

α/n^0 -only events identified via PID was prepared, and the $\alpha - \alpha$ coincidence events were selected using two criteria: We require the time interval between two consecutive α events to be less than 1 second, with energy selection within 5 standard deviations of the known α energies. The standard deviations are based on detector resolutions modeled using Gaussian functions, with the known α energies as the means.

Similarly, through α - α coincidence analysis, we obtained an activity of 0.012 ± 0.007 mBq/kg. In the Fig. 7, the time difference of selected $\alpha - \alpha$ coincidence events are represented as black dots with error bars. The coincidence time distribution was fitted by Eq. 4.1, with the half-life fixed at 140 ms; the fitted function is shown as a red line in Fig. 7. The contamination by ^{232}Th can be derived from the amplitude term of the best-fit model.

5 Summary and discussion

In COSINE-100, a dark matter search experiment, the unique LS veto system played a crucial role in background reduction and understanding. The next phase of COSINE-100, COSINE-100U, is under preparation, and LAB-based LS of 2400 L has been produced to use for the LS veto system. As part of the performance testing of the newly produced LS, the activities of ^{238}U and ^{232}Th , the main background elements, were measured.

A small-sized radiopurity screening detector was used for the test, with data collected over a 30-day period. Energy calibration of α events was performed by separating α/n^0 events from the β/γ sample. The $\beta - \alpha$ coincidence analysis of the sequential decays of ^{214}Bi and ^{214}Po in the ^{238}U decay chain provided measurements of internal contamination by ^{238}U and additional contamination by ^{222}Rn , resulting in a measured ^{238}U activity of 0.091 ± 0.042 mBq/kg. Additionally, the sequential α decays of ^{222}Rn and ^{216}Po in the ^{232}Th decay chain were identified, determining the ^{232}Th activity to be 0.012 ± 0.007 mBq/kg. These results are consistent with those of the liquid scintillator used in the COSINE-100 experiment, which reported activities of 0.087 mBq/kg and 0.016 mBq/kg for ^{238}U and ^{232}Th , respectively [11].

In order to check the influence of those measured activities on the background of the NaI(Tl) crystal, we invoked the background model of COSINE-100 [15]. The red histograms in Fig. 8 are

the background model of COSINE-100, while the contributions by ^{238}U and ^{232}Th contamination in the LS are shown in cyan and blue, respectively. One can see that the contributions are negligible for single-hit events in Fig. 8 (a), and the contribution at the region of interest (ROI) for WIMP extraction search (1-6 keV of single-hit events) is lower than 0.02 %. Hence we confirmed that the LS sample was sufficiently pure to be used as the veto system in the COSINE-100U experiment.

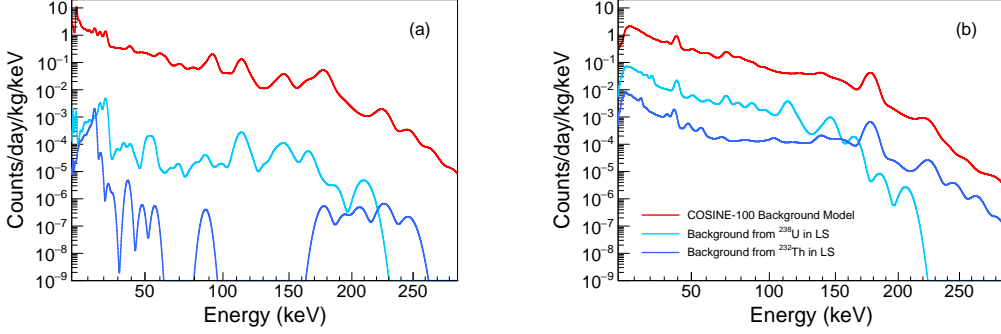


Figure 8. Simulated background model. The red histogram indicates the total COSINE-100 background model and the cyan and blue histograms indicate the contributions from ^{238}U and ^{232}Th contamination in LS, respectively. The single-hit energy spectrum (a) shows contributions of 0.07 %, while the multiple-hit spectrum (b) indicates contributions of 3.14 %. These low levels illustrate the minimal impact of LS contamination compared to the total COSINE-100 background model.

Activity measurements using HPGe detector For cross-validation, the radioactivities of the LS sample were also measured using a High Purity Germanium (HPGe) detector [16]. The HPGe detector collected data for 17.25 days at Yemilab. The results for four radionuclides are presented in Table 1, showing that all measurements were within the upper limits, indicating that the LS is sufficiently clean. Among these, the upper limit for ^{238}U includes the results of the measurement in this study.

Table 1. Radioactivity of the LS sample measured by HPGe detector

Nucleus	^{238}U	^{40}K	^{228}Ac	^{228}Th
Activity [mBq/kg]	< 0.90	< 7.39	< 2.01	< 0.74

Acknowledgments

This research was supported by: the Institute for Basic Science under project code IBS-R016-A1 Republic of Korea, the National Research Foundation of Korea (NRF) grant funded by the Korean government (MSIT) (NRF-2021R1A2C1013761), and the Chung-Ang University Research Scholarship Grants in 2023.

References

- [1] V.C. Rubin and W.K. Ford, *Rotation of the andromeda nebula from a spectroscopic survey of emission regions*, *The Astrophysical Journal* **159** (1970) 379.
- [2] D. Clowe, M. Bradač, A.H. Gonzalez, M. Markevitch, S.W. Randall, C. Jones et al., *A direct empirical proof of the existence of dark matter**, *The Astrophysical Journal* **648** (2006) L109.
- [3] PLANCK collaboration, *Planck 2013 results. XVII. Gravitational lensing by large-scale structure*, *Astron. Astrophys.* **571** (2014) A17 [[1303.5077](#)].
- [4] LUX-ZEPLIN collaboration, *First dark matter search results from the lux-zeplin (lz) experiment*, *Phys. Rev. Lett.* **131** (2023) 041002.
- [5] DAMA collaboration, *First results from DAMA/LIBRA and the combined results with DAMA/NaI*, *Eur. Phys. J. C* **56** (2008) 333 [[0804.2741](#)].
- [6] R. Bernabei et al., *Final model independent result of DAMA/LIBRA-phase1*, *Eur. Phys. J. C* **73** (2013) 2648 [[1308.5109](#)].
- [7] G. Adhikari et al., *Initial Performance of the COSINE-100 Experiment*, *Eur. Phys. J. C* **78** (2018) 107 [[1710.05299](#)].
- [8] N. Carlin et al., *COSINE-100 Full Dataset Challenges the Annual Modulation Signal of DAMA/LIBRA*, [2409.13226](#).
- [9] D.H. Lee et al., *COSINE-100U: Upgrading the COSINE-100 Experiment for Enhanced Sensitivity to Low-Mass Dark Matter Detection*, [2409.15748](#).
- [10] K.S. Park, Y.D. Kim, K.M. Bang, H.K. Park, M.H. Lee, J. So et al., *Construction of Yemilab*, *Front. in Phys.* **12** (2024) 1323991 [[2402.13708](#)].
- [11] G. Adhikari et al., *The COSINE-100 liquid scintillator veto system*, *Nucl. Instrum. Meth. A* **1006** (2021) 165431 [[2004.03463](#)].
- [12] COSINE-100 collaboration, *Improved background modeling for dark matter search with COSINE-100*, [2408.09806](#).
- [13] J. Park et al., *Production and optical properties of gd-loaded liquid scintillator for the reno neutrino detector*, *Nuclear Instruments and Methods in Physics Research Section A: Accelerators, Spectrometers, Detectors and Associated Equipment* **707** (2013) 45.
- [14] E. Sala, I.S. Hahn, W.G. Kang, G.W. Kim, Y.D. Kim, M.H. Lee et al., *Development of an underground low background instrument for high sensitivity measurements*, *J. Phys. Conf. Ser.* **718** (2016) 062050.
- [15] G. Yu et al., *Improved background modeling for dark matter search with COSINE-100*, [2408.09806](#).
- [16] E.K. Lee et al., *Measurements of detector material samples with two HPGe detectors at the Yangyang Underground Lab*, *PoS ICHEP2018* (2019) 809.